Cell Reports
Physical Science

CellPress
OPEN ACCESS

Article

The critical role of corrugated lamellae morphology on the tough mechanical performance of natural *Syncerus caffer* horn sheath

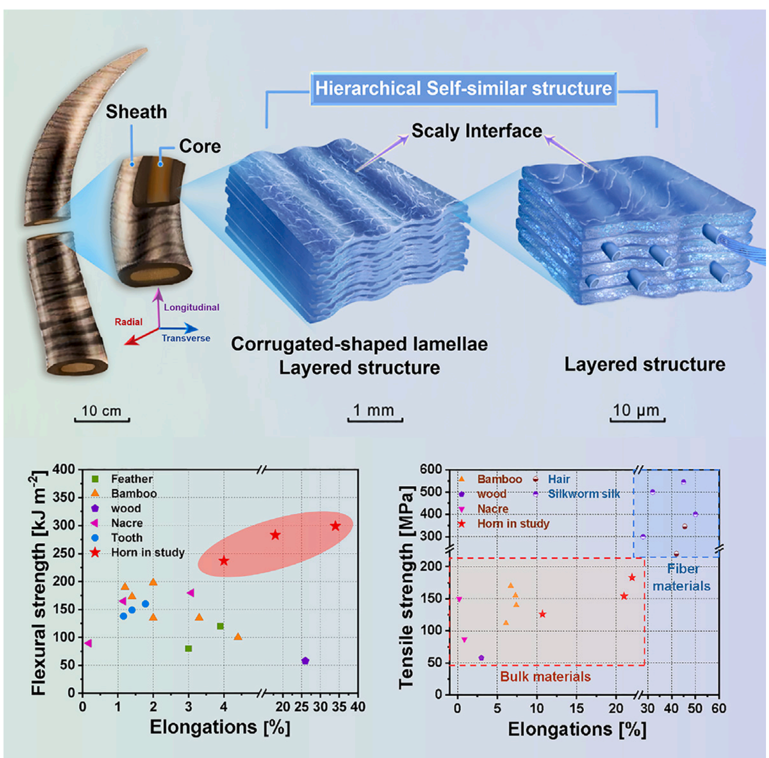

Yang et al. report that the *Syncerus caffer* horn sheath exhibits superior mechanical properties when compared with other bulk natural materials reported. The exceptional strength and toughness of the horn sheath can be attributed to the critical characteristics of its heterogeneous curved corrugated lamellae.

Kang Yang, Haotian Yu, Xinru Cao, ..., Wenhan Tian, Shihong Zhang, Robert O. Ritchie

juan.guan@buaa.edu.cn (J.G.)
zsh13637101221@163.com (S.Z.)
roritchie@lbl.gov (R.O.R.)

Highlights

Syncerus caffer horn sheath exhibits 183 MPa tensile strength

Heterogeneous corrugated lamellae in horn sheath leads to significant toughening effects

Uneven disulfide crosslink suggests an evolution of heterogeneous composition

Yang et al., Cell Reports Physical Science 4, 101576
September 20, 2023 © 2023 The Authors.
https://doi.org/10.1016/j.xcrp.2023.101576

Please cite this article in press as: Yang et al., The critical role of corrugated lamellae morphology on the tough mechanical performance of natural *Syncerus caffer* horn sheath, Cell Reports Physical Science (2023), https://doi.org/10.1016/j.xcrp.2023.101576

Cell Reports Physical Science

CellPress OPEN ACCESS

Article

The critical role of corrugated lamellae morphology on the tough mechanical performance of natural *Syncerus caffer* horn sheath

Kang Yang,[1,2] Haotian Yu,[1] Xinru Cao,[1] Juan Guan,[1,3,9,*] Siyu Cai,[4] Zexin Yang,[3] Wei Huang,[5] Bin Wang,[6,7] Nannan Qin,[1] Zihong Wu,[3] Wenhan Tian,[3] Shihong Zhang,[1,2,*] and Robert O. Ritchie[8,*]

SUMMARY

Horns from the *Bovidae* family represent extremely tough natural composites that resist flexural and impact damage during combat. However, the microstructure characteristics of these horns' sheaths and how this affects their mechanical properties remain to be explored. In this work, we report that the *Syncerus caffer* horn sheath exhibits the highest tensile strength of 183 MPa and fracture energy of 36.8 MJ m^{-3}, superior to other reported bulk natural materials. Comprehensive structure characterizations pin down the key factors of the horn sheath as the corrugated lamellae morphology. Finite-element modeling verifies that the critical characteristics of curved corrugated lamellae have a profound effect on the flexural and impact behavior. Furthermore, the ridge region for the highly curved lamellar morphology corresponds to greater disulfide crosslinking with ~2.6% sulfur, suggesting a purposeful evolution of the heterogeneous composition. This work aims to provide insights into the bio-inspired design of superior structural materials.

INTRODUCTION

The multi-scale structure and morphology of biological materials provides numerous inspirations for engineering synthetic materials.[1–4] One example of such natural materials are animal horns from the *Bovidae* family, which are often subjected to bending and impact loading during combat. The horned animals comprise cloven-hoofed, ruminant mammals that include cattle, bison, buffalo, antelopes, and caprines. As these animals only possess one set of horns throughout their individual lifetimes, and as a broken horn cannot be naturally restored, the horn has evolved with characteristic damage resistance.[5–7] As an example, the buffalo horn consists of a bony core and an outer skin layer called the horn sheath.[8] The core is usually dissected into proximal, middle, and distal sections, whereas the sheath consists of a keratin-based protein material that possess both strength and toughness to withstand extreme loads.[8,9] The nanoscale conformation structure with high-density hydrogen bonding and disulfide crosslinking contributes to the strength and stiffness of the sheath.[6,8] At the microscale, the strength and toughness of horns as natural materials is significantly reduced upon hydration.[10–12] Interestingly, such a hydration effect on the horn sheath can be utilized to make "smart" shape-memory materials.[13] At the macroscale, lamellar buckling and delamination, along with extrusion densification, have been shown to enhance the toughness during compression and impact loading of the horn.[14–16]

In phylogeny, the *Bovidae* family can be divided into sub-families *Bovinae*, *Caprinae*, and *Antilocapridae*. Tubular structures mainly exist in the horn of bighorn

[1]School of Materials Science and Engineering, Anhui University of Technology, Maanshan 243002, China

[2]Key Laboratory of Green Fabrication and Surface Technology of Advanced Metal Materials (Anhui University of Technology), Ministry of Education, Maanshan 243002, China

[3]International Research Center for Advanced Structural and Biomaterials, School of Materials Science and Engineering, Beihang University, Beijing 100191, China

[4]Guiyang Engine Research Institute of Aviation Industry Corporation of China (AVIC), Guiyang 550081, China

[5]School of Materials Science and Engineering, Huazhong University of Science and Technology, Wuhan 430074, China

[6]Department of Mechanical Engineering, City University of Hong Kong, 83 Tat Chee Avenue, Kowloon, Hong Kong, China

[7]Shenzhen Institute of Advanced Technology, Chinese Academy of Sciences, Shenzhen 518055, China

[8]Department of Materials Science & Engineering, University of California, Berkeley, Berkeley, CA 94720, USA

[9]Lead contact

*Correspondence:
juan.guan@buaa.edu.cn (J.G.),
zsh13637101221@163.com (S.Z.),
roritchie@lbl.gov (R.O.R.)

https://doi.org/10.1016/j.xcrp.2023.101576

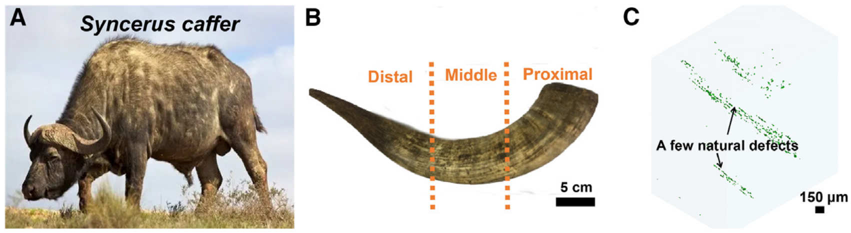

Figure 1. Images of *Syncerus caffer* and its horn
(A) Photographic image of *Syncerus caffer*.
(B) Photographic image of *Syncerus caffer* horn.
(C) X-ray microcomputed tomography (μ-CT) image of horn sheath sample. Green colored dots represent defects in *Syncerus caffer* horn.

sheep, which belong to *Antilocapridae*. For this sub-family, the highly anisotropic fibrous and tubular structure of the horn sheath has been ascribed to contribute to its excellent mechanical properties, especially energy absorption.[17,18] The *Antelope* horn sheath is considered to represent a typical short-fiber reinforced composite whose mechanical properties upon hydration can be predicted using a modified Voigt estimate of composite stiffness.[19] The interlaminar fracture toughness of this sheath composite can be improved with fibers across the neighboring lamellae.[20] The tubular structure of the horn of bighorn sheep has been claimed to generate significant toughness and energy absorption by promoting crack tortuosity and tubule collapse[21,22]; oriented tubules have been shown to improve the resistance to damage in both solid rhinoceros horn and hollow bighorn sheep horn.[23] Similar tubular structures are found in horse hoof, antler, and tooth and act to provide enhanced toughness in these materials.[24–27]

Corrugated lamellae have been a critical morphology feature in *Bovinae* horn sheath and are claimed to contribute to their superior mechanical performance.[15,28] However, there have been few systematic studies and quantitative evaluations of the explicit effect of the corrugated lamellae structure, especially under both quasi-static and impact loading conditions. Presumably, it is challenging to extricate the specific role of the corrugated lamellae morphology from the other structural features such as the nanoscale conformation structure and the fibrous morphology. Coincidentally, corrugated lamellae have also been found in seashells such as *Clinocardium* spp. and *Odontodactylus scyllarus*, proven to contribute to the high toughness of the shells.[29,30] With respect to bio-mimicry, bio-inspired corrugation-shaped structures across multiple length scales have been designed[29,31] into synthetic materials. For example, wavy/corrugated interfaces of composites promoted stronger interfacial adhesion, and dovetail structures enhanced crack deflection during the fracture process.[32] Moreover, laminate composites involving wavy or interlocked interfaces achieve considerably improved impact resistance compared with those with traditional flat interfaces.[33] Accordingly, the intent of the current work is to present an in-depth study of the characteristics of corrugated lamellae in natural *Bovinae* horn sheath to discern the relationship between such microstructure architectures and their toughness effect.

To achieve this objective, we select the *Syncerus caffer* horn sheath, shown in Figure 1, as a representative *Bovinae* horn sheath. Notably, our initial exploration includes three distinct types of horn sheaths from *Syncerus caffer*, Qinghai Yak, and domestic cattle, as vividly portrayed in Figure S1. Among the three horn sheath materials, the *Syncerus caffer* horn sheath exhibits notably superior mechanical

Cell Reports
Physical Science
Article

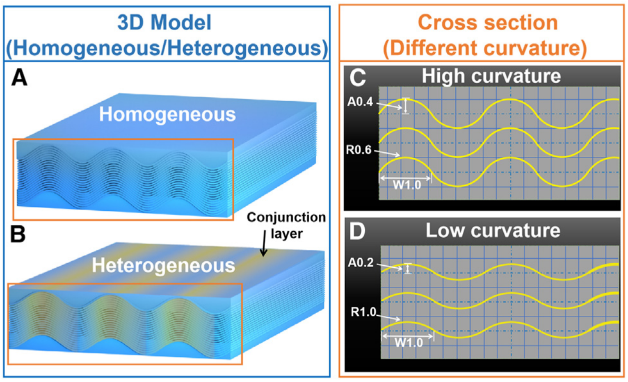

Figure 2. Layered structure model
(A) 3D models of homogeneous layered structure.
(B) 3D models of heterogeneous layered structure.
(C) Models with parameter settings for high curvature.
(D) Models with parameter settings for low curvature. Parameters: wavelength (*W*), amplitude (*A*), and radius (*R*).

properties (as evidenced in Figure S2). The 3D structure from microcomputed tomography (micro-CT) indicates that the *Syncerus caffer* horn sheath possesses primarily a dense structure, as opposed to being porous or featuring a tubular structure. Consequently, we concentrate on studying the *Syncerus caffer* horn sheath. It is used as a model material (Figure 2) to reveal the toughening mechanisms associated with the microstructure of corrugated lamellae. Experimental and simulation methods are combined to investigate the deformation to failure processes under tensile, flexural, and impact loading. We believe that this work can offer new insights into the design of tough structural materials for applications where toughness properties are critical requirements.

RESULTS

Multi-scale structure of *Syncerus caffer* horn sheath

Earlier research proposed that the multi-scale structure characteristics of the horn sheath contribute to such superior tensile and flexural strength and toughness.[1,34] Here, we illustrate the multi-scale structure of the *Syncerus caffer* horn sheath (Figure 3) to reveal the detailed structure of the lamellae and its relationship to the fracture morphologies by breaking open the fractured samples in liquid nitrogen. The fracture morphologies of the transverse and horizontal directions, shown in Figures 3D and 3E, respectively, reveal the keratin microfibers as the reinforcement within each lamellae. The snap-back fracture morphology of the fiber indicates the tough behavior of the *Syncerus caffer* horn sheath after the liquid nitrogen treatment.

X-ray diffraction (XRD), differential scanning calorimetry (DSC), and Fourier transform infrared (FTIR) analyses in Figures S3 and S4 can indicate the differences in the keratin structure of three sections of the horn sheath. XRD results in Figure S3A showed little variation among the distal, middle, and proximal sections. The calculated crystallinity values across the three locations were very similar, approximately 7.5%. Despite that horn sheaths from different species may have highly variable conformation structures,[35] the three sections from *Syncerus caffer* horn sheath exhibited very similar conformation structure (~25% β-sheet) in Figure S4B. The conformation contents were calculated using the software Peakfit from the Gaussian function fit to the Amide I region (1,600–1,700 cm^{-1}) according to an established

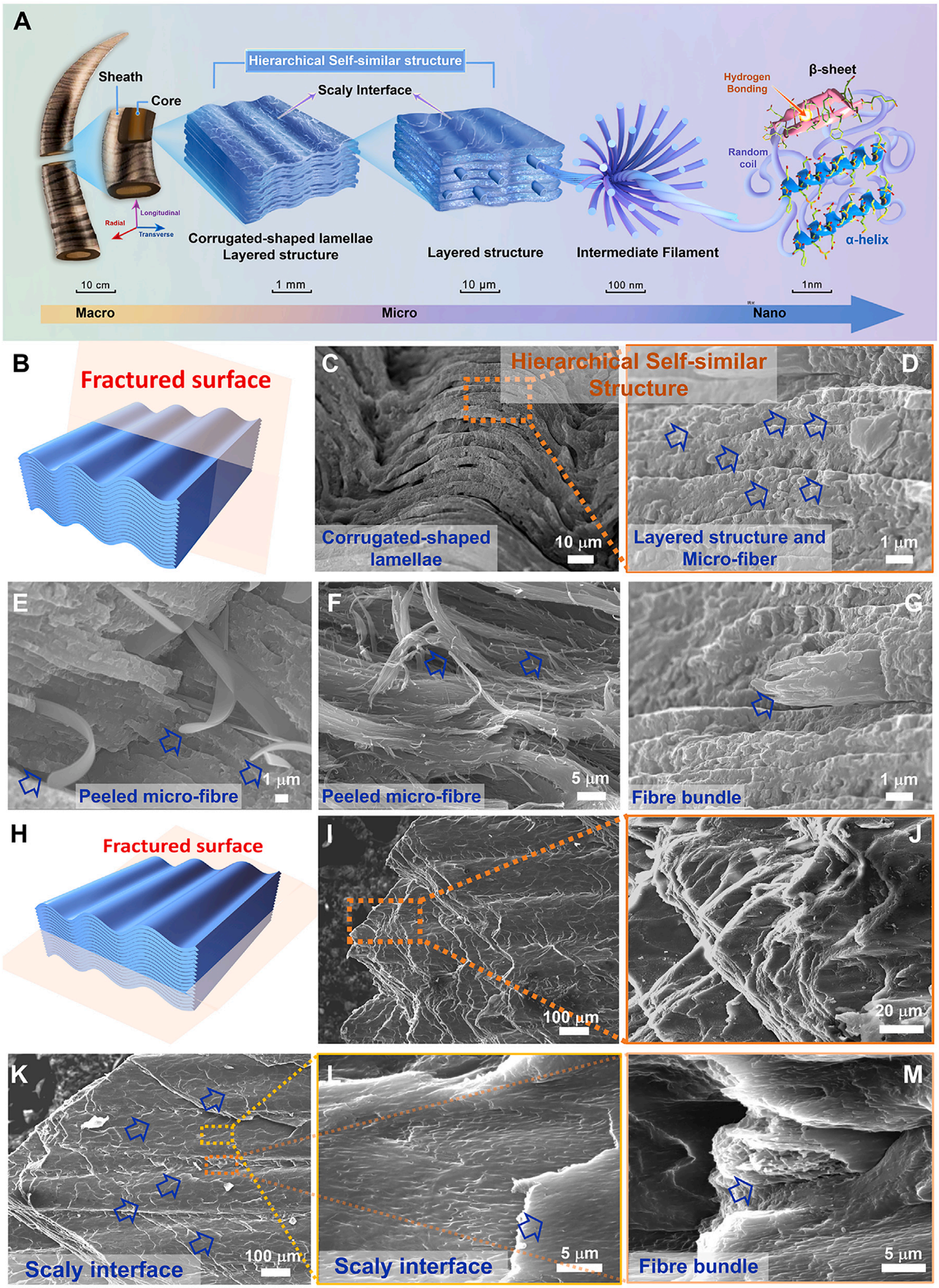
A
Hierarchical Self-similar structure
Sheath
Core
Scaly Interface
Hydrogen Bonding
β-sheet
Random coil
α-helix
Longitudinal
Radial
Transverse
Corrugated-shaped lamellae
Layered structure
Layered structure
Intermediate Filament
10 cm
1 mm
10 μm
100 nm
1nm
Macro
Micro
Nano
B
Fractured surface
C
Hierarchical Self-similar Structure
D
Corrugated-shaped lamellae
10 μm
Layered structure and Micro-fiber
1 μm
E
F
G
Peeled micro-fibre
1 μm
Peeled micro-fibre
5 μm
Fibre bundle
1 μm
H
Fractured surface
I
J
100 μm
20 μm
K
L
M
Scaly interface
100 μm
Scaly interface
5 μm
Fibre bundle
5 μm

Figure 3. Multi-scale structure of *Syncerus caffer* horn sheath

(A) Schematic diagram of multi-scale structure characteristics of *Syncerus caffer* horn.

(B–M) Lamellae model representation (B and H) and SEM images (C–G and I–M) of transverse microstructural characteristics (B and C–G) and horizontal microstructural characteristics (H and I–M) in *Syncerus caffer* horn sheath. All the microstructure images were procured following brittle fracture of samples in liquid nitrogen. In the SEM images, blue arrows designate specific features including layered structure, microfiber, peeled microfiber, scaly interface, and fiber bundle, as itemized in the bottom left corners.

method.[36] Furthermore, the DSC curves in Figure S3B indicated very similar structure changes among the three sections during the heating until the degradation. Such results suggest that the condensed structure at the nanoscale should not constitute the key variant to suffice the significant differences in the sectional mechanical properties of the *Syncerus caffer* horn sheath.

Mechanical properties of the *Syncerus caffer* horn sheath

The tensile and flexural stress-strain curves of the dehydrated *Syncerus caffer* horn sheath material are shown in Figures 4A and 4B, with the fracture strength, elongation, and fracture energy values summarized in Figures 4C and 4D. Among the three sections, the distal specimens exhibited the highest tensile strength (183 MPa) and flexural strength (299 MPa) and also displayed the highest tensile fracture energy (36.8 MJ m^{-3}) and flexural fracture energy (60.4 MJ m^{-3}). From the distal to the proximal sections, the tensile/flexural strength decreased together with the elongation and fracture energy. Specifically, an after-yield plateau can be seen in the stress-strain curves of the distal/middle specimens, which achieved a high tensile elongation of $\sim$25% (Figure 4A). The maximum flexural strain of the distal specimen was $\sim$30% (Figure 2B). Similar trends of decrease from distal to proximal were seen in the mechanical strength and elongation of the fully hydrated groups (Figure S5).

In addition, we conducted flexural tests to evaluate the performance of the transverse orientation for comparison. As shown in Figure S6, the bending properties of the *Syncerus caffer* horn sheath in the transverse direction showed similar trends to those observed in the longitudinal directions. The distal part exhibited the highest flexural strength, measuring approximately 299.9 MPa. These findings emphasize the enhanced mechanical performance of the curved lamellae morphology in both longitudinal and transverse directions.

It is important to note that the measured densities for the proximal, middle, and distal sections were 1,250, 1,280, and 1,290 kg m^{-3}, respectively. For each sample, we quantified the specific tensile and flexural strength, as illustrated in Figure S7. The trends of specific tensile and bending strength values from proximal to distal sections resemble those of tensile/bending strength values. Additionally, thermogravimetry (TG) analysis in Figure S3C revealed that the residual inorganic/mineral contents post-carbonization were quite similar across all three sections, at roughly 42.5% at 400°C. These findings suggest that density and mineral content do not constitute key factors influencing the sectional mechanical properties.

Figures 4E and 4F provide a comparison of the tensile and flexural strength of various dry horn sheath materials studied in this work with those previously published in the literature.[5,6,9,20,22,28] Most data of three *Syncerus caffer* horn sheath materials from this work lie in the upper right corner, demonstrating excellent strength and elongation properties.

Fracture morphologies of the *Syncerus caffer* horn sheath

The microstructures of the three sections of the horn sheath are shown in Figures 5B–5D. The distal and middle regions display more corrugated lamellae structure compared

CellPress
OPEN ACCESS

Cell Reports
Physical Science
Article

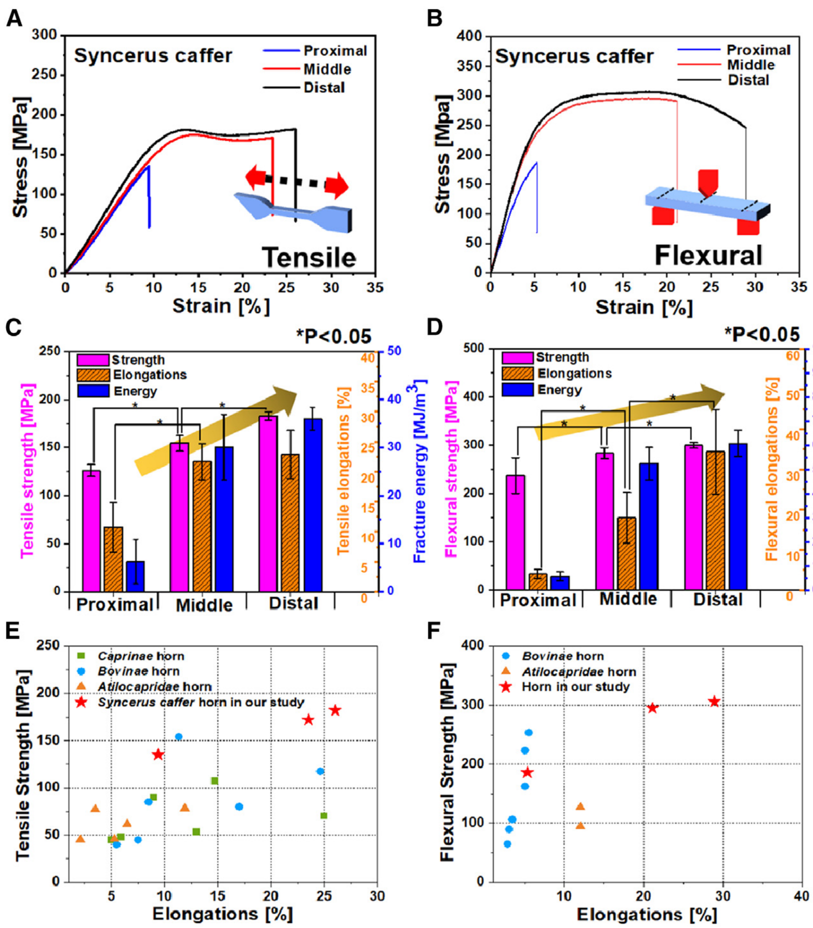

Figure 4. Mechanical properties of dry *Syncerus caffer* horn sheaths

(A) Tensile stress-strain curves.

(B) Flexural stress-strain curves.

(C) Tensile strength and elongation derived from the tensile stress-strain curves.

(D) Flexural strength and elongations derived from the flexural stress-strain curves.

(E and F) Comparison of measured (E) tensile strength and (F) flexural strength versus elongation for dry horn sheath materials with literature values.[5,6,9,20,22,28]

The error bars represented in (C) and (D) are based on standard deviations. P value represents the probability that there is no significant difference between the two groups. P value represents tprobability that there is no significant difference between the two sets of test results.

with the nearly flat-shaped lamellae in the proximal part, suggesting a gradual change in curvature of the lamellae along the direction of growth. Simplified models of the varied curved lamellae structures at the three positions are illustrated in Figures 5E–5G. The two parameters to define the corrugation in the lamellae are the wavelength (*W*) and amplitude (*A*), and the *W*/*A* ratio directly reflects the degree of curvature. *W*/*A* is estimated to be ~4 for the distal section (Figure 5G) and ~6 for the middle section (Figure 5F). A lower value of *W*/*A* here represents a higher degree of curvature.

The macroscopic morphologies in Figures 5H–5J reveal that the highly curved corrugated lamellas correspond to a complex crack path in the distal part. Unlike the single crack in the proximal sample denoting a catastrophic fracture, the crack in the distal part undergoes multiple deflections. Furthermore, the fracture morphologies along the lateral direction in Figures 5K–5M reveal multiple layered fractures and a scaly fracture pattern (highlighted in colored dashed lines) in the distal

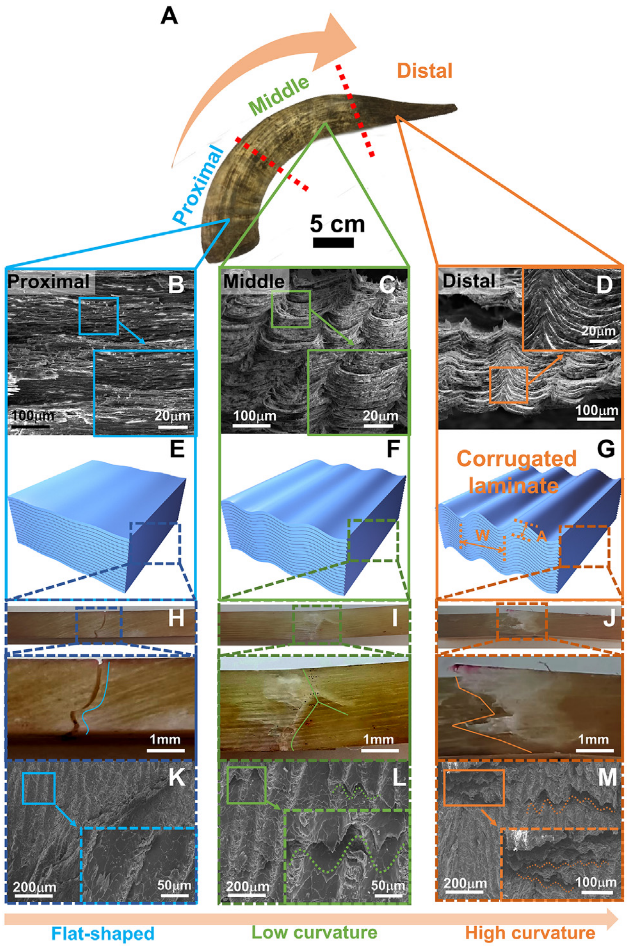

Figure 5. Fracture morphologies after tensile/flexural tests

(A) Photographic image of *Syncerus caffer* horn and the three sections.

(B–D) SEM morphology of fractured surfaces of the (B) proximal, (C) middle, and (D) distal regions.

(E–G) Lamellae structure models of the (E) proximal, (F) middle, and (G) distal regions.

(H–J) Photo images of the fractured flexural specimens from side views for the (H) proximal, (I) middle, and (J) distal regions.

(K–M) Corresponding SEM images along the lateral direction inside the fractured flexural specimens for the (K) proximal, (L) middle, and (M) distal regions of the *Syncerus caffer* horn sheath.

part. These fracture morphologies suggest a correlation between corrugated structure and crack deflections. Additionally, secondary deflections of the major crack was detected in the single-edge notched specimen under three-point bending (Figure S8).

To comprehensively understand the effect of corrugation, we further studied the distal specimens of the horn sheaths from Qinghai yak and domestic cattle (Figure S1). The stress-strain curves and derived properties in Figure S2 showed that the domestic cattle horn sheath displayed the lowest strength and elongation. Microstructure analysis in Figure S9 revealed that the Qinghai yak samples possessed clear corrugations in their lamellae structure, whereas we only observed a nearly flat-shaped lamellae structure in the domestic cattle samples. These results further supported our contention that the corrugation in lamellae is related to the mechanical strength and toughness of horn sheath materials.

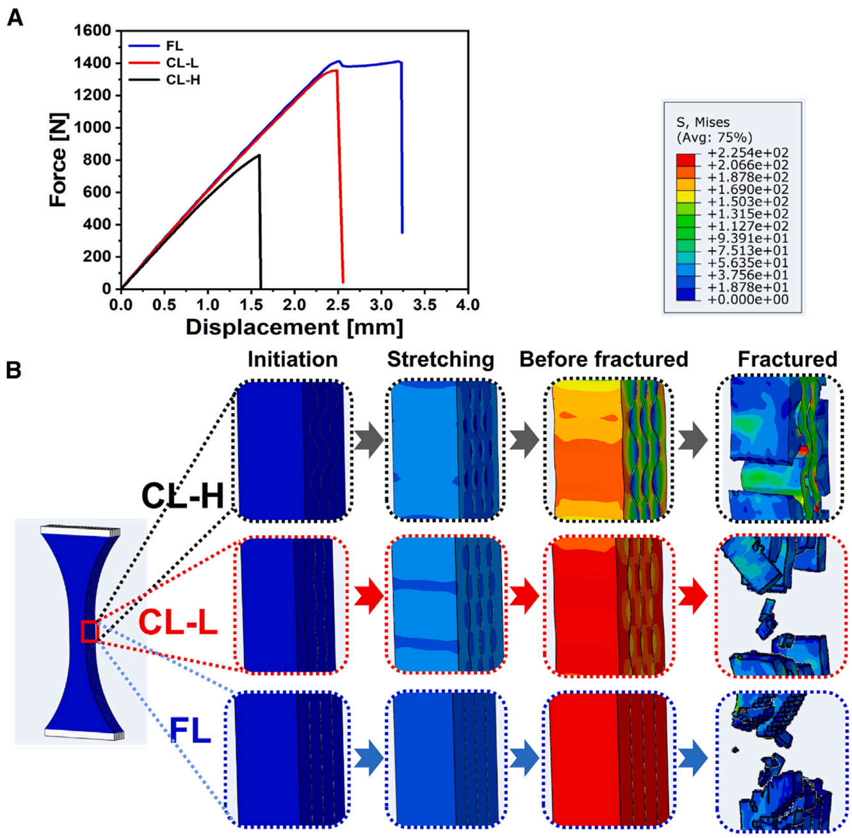

Figure 6. Simulation results from the layered corrugated lamellae models without a heterogeneous conjunction layer under tensile loading

(A) Tensile force-displacement curves of flat-shaped lamellae (FL), corrugated lamellae with low curvature (CL-L), and corrugated lamellae with high curvature (CL-H).

(B) Stress nephogram and fracture characteristic of FL, CL-L, and CL-H during the tensile deformation.

Modeling of the effect of corrugation on the mechanical behavior of the horn sheath

To explore the effect of corrugation quantitatively, models based on the finite-element method (FEM) were constructed (Figures 2, 6, and S10). An elastoplastic constitutive relationship was used to describe the stress-strain behavior of the horn sheath based on a lamellae model.[37] Previous FEM studies have focused on the conical structure of the whole horn and the porous bone core,[38–40] whereas the simulations in the present work are centered on the corrugated structure of the *Bovinae* horn sheath.

First, three simple models were established including flat-shaped lamellae (FL) and lamellae with low curvature (CL-L) and high curvature (CL-H). The models were subject to various loading modes involving tensile, flexural, and drop-weight impact. Under the tensile mode, the FL model yielded the highest strength and toughness (Figure 6B). Interestingly, the CL-L model for low-curvature corrugated lamellae exhibited a tensile strength similar to that for the FL model but that was ~60% higher than that of high-curvature model CL-H. Such results imply that the corrugations in lamellae would appear to impair the mechanical properties, which is inconsistent with the experimental results mentioned above. The tensile stress diagram and

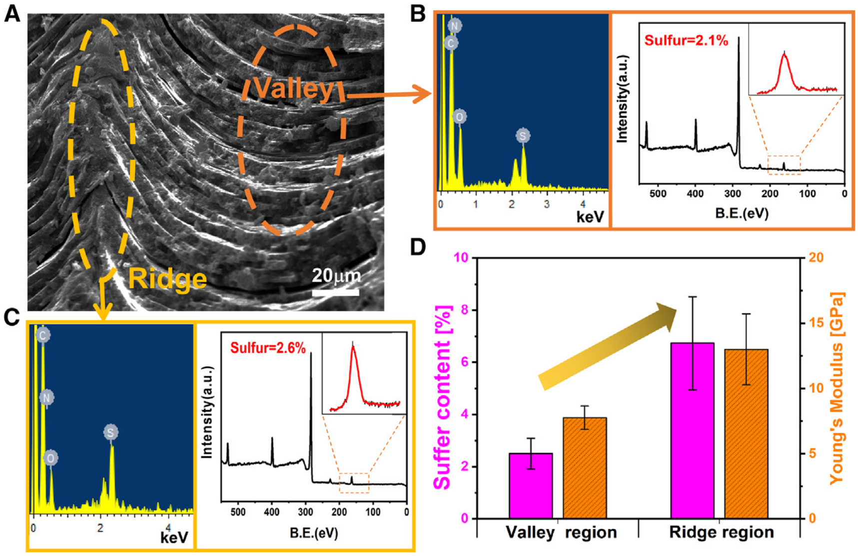

Figure 7. Analysis of heterogeneous corrugated structure

(A) SEM image of the microstructure of distal part in *Syncerus caffer* horn sheath.

(B) Element analysis of sulfur from EDS spectra and XPS in the valley region.

(C) Element analysis of sulfur from EDS spectra and XPS in the ridge region.

(D) Content of sulfur derived from XPS analysis and modulus values from nanoindentation tests for the valley and ridge regions.

The error bars represented in (D) are based on standard deviations.

fracture morphologies in Figure 6C showed that the corrugated structure induced a non-uniform stress field, with the resulting severe stress concentrations leading to premature catastrophic failure.[41] The stark discrepancy between the experimental observations and the results of this numerical analysis establish that such a simple model of the corrugated lamellae is inadequate to simulate the superior mechanical performance of *Syncerus caffer* horn sheath.

Biologically, horn is formed through processes of cell proliferation, cornification, and keratinization under natural conditions.[42] In the basal layer of the epidermal tissue, basal cells grow and proliferate in small vessels, then transform to the stratum corneum cell type, marked by keratin filament aggregation and the formation of intermolecular disulfide crosslinks.[43] Presumably, cell differentiation from epidermal cells to keratinocyte may generate non-uniform/-heterogeneous corrugated lamellae. A formation mechanism for the structure in *Syncerus caffer* horn sheath with keratin aggregation is illustrated in Figure S11. Such cell differentiation processes can be affected by external stresses, as Wolff's Law proposes for bone osteocyte during growth.[44,45] As the ridge region of the corrugated lamellae usually experiences greater stresses,[46] it may promote keratinization and produce more keratinocytes.

Evidently, we performed qualitative/semi-quantitative analysis of the sulfur content at different locations using scanning electron microscopy (SEM) and energy-dispersive spectroscopy (EDS) spectra in Figure 7. The analysis revealed that the ridge region of the corrugated lamellae structure exhibited a higher sulfur content compared with the valley region. To further quantify the sulfur content, X-ray photoelectron spectroscopy (XPS) analysis was also employed. The results in Figures 7B and 7C confirmed that the sulfur content varied from a maximum of 2.6% at the ridge to a minimum of 2.1% at the valley. Additionally, we conducted nanoindentation tests to assess the local modulus of the ridge and valley regions, as shown in

CellPress
OPEN ACCESS

Cell Reports
Physical Science
Article

Figures S12 and 7D. The results demonstrated that the ridge region exhibited a much higher indentation modulus of 12.5 GPa than the 4 GPa of the valley region. Such results of XPS, EDS spectrum, and nanoindentation experiments indicate a higher degree of keratinization and crosslinking and thus rigidity in the ridge region, consistent with the above proposed formation mechanism. In light of the biological mechanism, the models were amended to incorporate the heterogeneous chemical structure of the keratinization of the horn sheath structure, shown in Figure 2B.

Based on considerations described above of the formation of the heterogeneous corrugated lamellae structure with keratin fibers at the ridge region, modified models with a conjunction layer (C) were further developed to simulate the greater degree of keratinization at the ridge region in the *Syncerus caffer* horn sheath, as illustrated in a schematic diagram in Figure 8; these are termed FL-C, CL-L-C, and CL-H-C, respectively, for flat-shaped lamellae and for lamellae with low curvature and with high curvature, respectively, all with a conjunction layer. At the ridge region of the distal horn sheath with greater curvature, the conjunction layers are taken to have a higher stiffness and lower ductility. Consequently, based on the predicted force-displacement curves in Figures 8A and 8B, the CL-H-C model showed the highest strength and toughness (Figure 8A), which corresponds well with the experimental results. According to the fracture surfaces in Figure 8C, the CL-H-C model displayed local ductile fracture characteristics, which were absent in the results from the FL-C and CL-L-C models. This illustrates that the toughening effect is exerted by the corrugation and the heterogeneous designs in the lamellae structure.

Furthermore, simulations under three-point bending mode in Figures 8B and 8D showed that the corrugated lamellae structure exhibits superior mechanical performance to the flat-shaped lamellae structure. However, the addition of the conjunction layer only marginally affected the results (c.f. Figures 8B and S9). This implies that the corrugated lamellae are more advantageous for elevating the flexural stiffness and toughness. The rough fracture morphologies of the corrugated lamellae shown in Figure 8D also confirmed that the corrugations can induce crack deflection, which serves to enhance the extrinsic toughness. However, if the degree of curvature is excessive, greater incipient damage appears to reduce the plasticity due to stress concentration.

To further investigate the effect of interfacial adhesion between lamellae, a new set of models were constructed to incorporate an enhanced interface layer between lamellae. Simulations under tensile and three-point bending modes in Figures S13 and S14 show that lamellae with greater interfacial strength do improve the efficiency of the strengthening and toughening of the corrugated lamellae.

DISCUSSION

As shown in Figures 4E and 4F above, the *Syncerus caffer* horn sheath exhibits excellent strength and toughness among all kinds of horn sheaths. Particularly, the *Syncerus caffer* horn sheath exhibits both high strength and high ductility, which are often mutually exclusive properties for many materials.[4] Further, we compare the tensile and flexural properties of the *Syncerus caffer* horn sheath with other natural materials, as depicted in Figure 9. The results suggest an unparalleled superiority of horn sheaths in terms of flexural properties, displaying exceptional strength and elongations that surpasses all other bulk natural materials. When assessing tensile properties, the strength and toughness of the *Syncerus caffer* horn sheath outdo all other bulk natural materials but fall slightly behind fibrous materials like spider silk. This discrepancy is attributed to the size effect. Hence, it is reasonable to

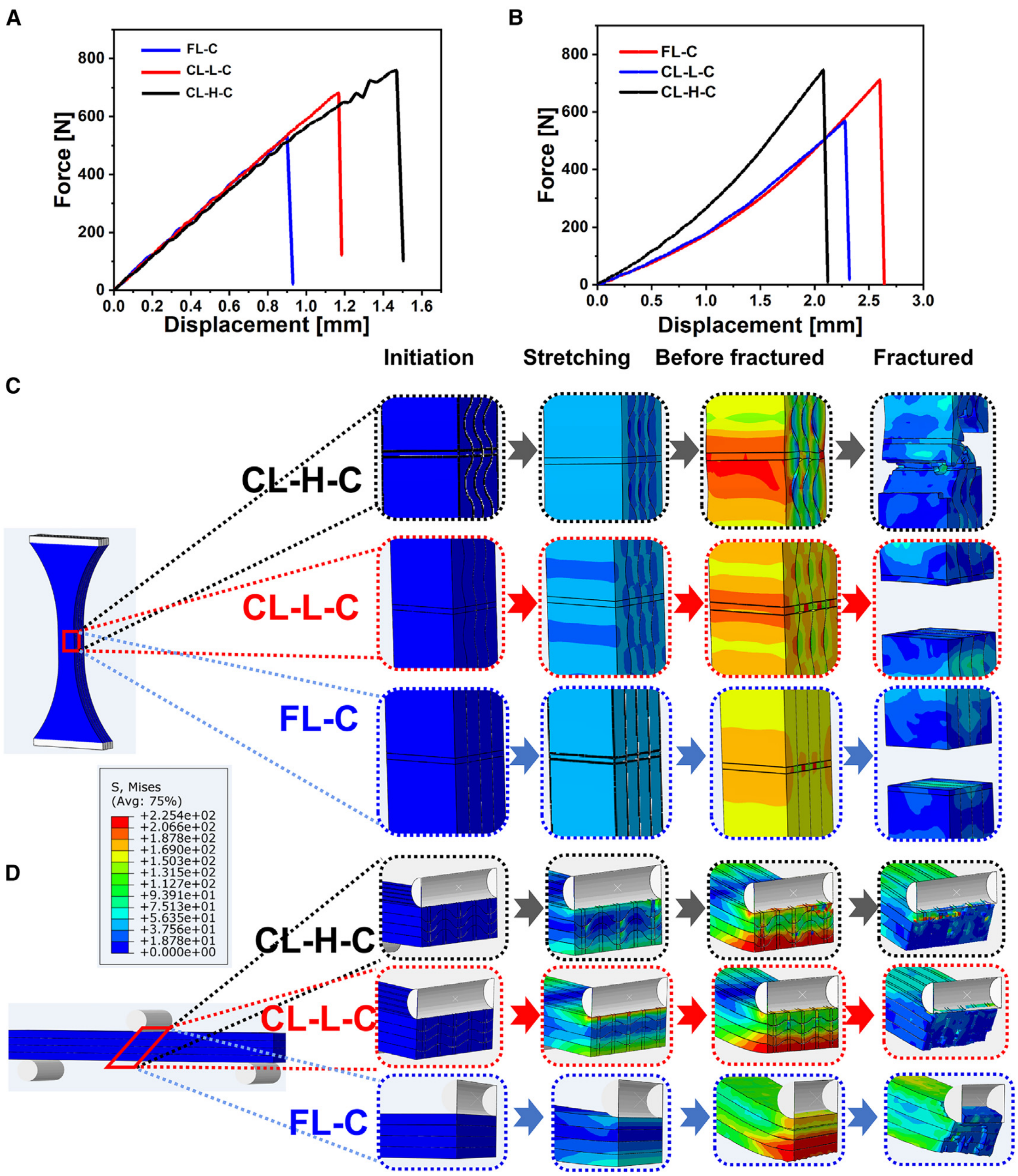

Figure 8. Simulations of corrugated lamellae models with heterogeneous conjunction layer under tensile and flexural loading

(A and B) Tensile (A) and flexural (B) force-displacement curves from the FL-C, CL-L-C, and CL-H-C models.

(C and D) Stress nephogram and fracture characteristics of the tensile (C) and flexural (D) tests.

conclude that the *Syncerus caffer* horn sheath stands out as the most formidable in terms of strength and toughness among all identified natural bulk materials. A deep understanding of its toughening mechanism can greatly facilitate the development of high-performing bio-inspired materials.

To unravel the primary toughening mechanism within the *Syncerus caffer* horn sheath, we examine the density, mineral content, crystallinity, conformational structure, and morphology of the proximal, middle, and distal sections, as detailed in Figures 5, S3, and S4. The analysis reveals negligible differences in density,

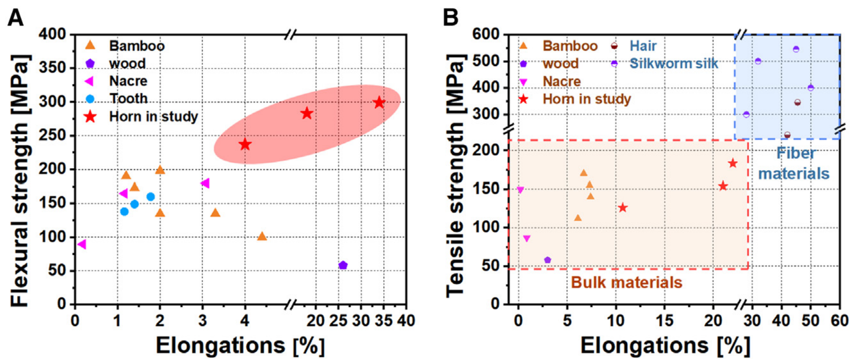

Figure 9. Comparison of mechanical properties between *Syncerus caffer* horn and other natural materials

Tensile (A) and flexural (B) properties of various representative natural materials[47–56] in comparison with the *Syncerus caffer* horn sheath from our study.

composition, and nanostructure across these positions. However, stark contrasts emerge in the corrugated morphology of the microstructure. Notably, the distal section, marked by a superior *W/A* ratio in its corrugated structure, registered the highest values for both specific tensile strength (around ~141.5 kPa/kg m^{-3}) and specific flexural strength (approximately 232 kPa/kg m^{-3}). Consequently, through a method of elimination, we pinpoint the corrugated structure as the probable pivotal toughening structure within the *Syncerus caffer* horn sheath.

The fracture morphology and crack propagation observed post-flexural experiment further substantiate the effect of the corrugated structure (Figure 5). As previously mentioned, the presence of multiple deflections and a phased fracture pattern in the distal section imply a link between the corrugated structure and crack deflection. Indeed, these cracks are in directions perpendicular to the plane of maximum tensile stress in the flexural sample, indicating very large crack deflections ~90° along the longitudinal direction. These crack deflections by the greater curvature of the corrugated lamellae structure with greater curvature can locally elevate the toughness in the longitudinal direction by a factor of almost 2. Usually, the two important factors dictate the crack deflection: the plane of maximum tensile stress and the path of weakest microstructure.[57] The corrugated lamellae with laterally asymmetric shapes and heterogeneous compositions can lead to varied regional stiffness in *Syncerus caffer* horn sheath. This infers that corrugations can lead to more crack deflections and hence a tougher behavior.

By utilizing finite-element simulation, it was observed that the corrugated structure model's mechanical simulation results align with flexural experiments but deviate in the tensile experiments. By analysis with SEM, XPS, and EDS, we pinpoint a heterogeneous corrugated structure within the *Syncerus caffer* horn sheath, characterized by local stiffening at the ridge region. Based on these findings, we optimize the corrugated structure model, leading to simulation results that mirror experimental data. This comparative approach between experimental and simulation studies deepens our grasp of the heterogeneous corrugated structure. We thus establish a compelling correlation between the locally enhanced corrugated stiffness and the mechanical performance.

The strengthening and toughening effect of corrugated structures has been explored in previous research. We categorize the examined corrugated structures into distinct features, as delineated in Table S1. Firstly, the waviness structure in nacre is predicated on separate inorganic tablets, not on a continuous phase, resulting in strain hardening and transverse expansion as primary toughening mechanisms.[58,59] Secondly, suture structures in the diabolical ironclad beetle and boxfish are rooted in the fusion of dissimilar materials, where mechanical interlocking plays a crucial role.[60,61] Thirdly, the wavy layer stacking structure, consisting of rigid inorganic and ductile organic phases, significantly enhances toughness.[29,62] Lastly, nanoasperity denotes feature points on the nacre interface that deter interface slippage, even though they do not form a complete corrugated structure.[63] Of the various corrugated and corrugated-like structures described, the wavy layer stacking structure closely echoes the internal corrugated configuration found in the *Syncerus caffer* horn sheath, according to our findings. Both structures feature continuous corrugated layers but diverge in two main aspects: firstly, the *Syncerus caffer* horn sheath deviates from the typical overlapped layer structure of rigid inorganic and pliant organic phases, consisting predominantly of keratin, an organic compound. Secondly, our study highlights that the valley and ridge regions of the corrugated structure possess a heterogeneous composition, where the increased rigidity at the ridge region enables key strengthening and toughening effects. Based on the fracture morphology observations and simulations conducted herein, we ascertain that local stiffening is essential in corrugated morphologies exhibiting a heterogeneous structure. This could further enhance transverse expansion, facilitate crack deflection, and construct intricate fracture pathways.

The *Syncerus caffer* horn sheath exhibits superior mechanical properties among the horn sheath materials, with ~183 MPa tensile strength, ~299 MPa flexural strength, and ~36.8 MJ m^{-3} tensile fracture energy. The distal, middle, and proximal sections of the *Syncerus caffer* exhibit varied mechanical properties, proposed to be highly correlated to varied corrugation morphology. Finite-element modeling verifies that the corrugated lamellae structure can exert significant strengthening and toughening effects under tensile, flexural, and impact loading conditions. The heterogeneous structure stemming from the biological keratinization process also plays a critical role within the corrugations to achieve the strengthening effect. Such a close correlation between the heterogeneously corrugated lamellae structure and superior toughness should inspire new designs of super-tough structural materials.

Although the effect of corrugated lamellae structure on the mechanical properties of *Bovinae* horn sheath has been explored in this work, some questions remain unresolved. Specifically, it remains uncertain whether the corrugated lamellae structure operates effectively for different *Bovinae* horn species under various impact loads, which is a recognized advantage of the horn.[64] Future studies on *Bovinae* horn sheath are therefore warranted, which will hopefully shed light on the comprehensive design principles of new structural materials with superior damage tolerance.

EXPERIMENTAL PROCEDURES

Resource availability

Lead contact

Further information and requests for resources and reagents should be directed to and will be fulfilled by the lead contact, Prof. Juan Guan (juan.guan@buaa.edu.cn).

CellPress OPEN ACCESS

Cell Reports Physical Science
Article

Materials availability

All stable and unique materials generated in this study are available from the lead contact upon reasonable request.

Data and code availability

All of the data supporting this study have been shown in the article and supplemental information. Other related data are available from the corresponding author upon reasonable request.

Materials

The *Syncerus caffer* horns studied in this work were obtained from a slaughterhouse in Anhui Province, China. Five fresh horns from different adult and healthy animals were chosen to avoid any variability in age or disease. The sheath specimens were conditioned to remove moisture and to achieve the same dry state. Specifically, all specimens were treated in an oven at ~100°C for 48 h. Fully hydrated *Syncerus caffer* horn specimens were also prepared by immersing the samples in phosphate-buffered saline (PBS) solution (0.01 M) for 2 days prior to testing. Orientations and positions were carefully controlled to minimize the non-focal structure variations. The long side of the majority of specimens in this work was along the growth direction/longitudinal orientation of the horn. Due to the small dimensions (<5 mm) along the radial direction, only a limited number of specimens could be obtained for the transverse and radial orientations. Sectional specimens were prepared from the proximal, middle, and distal sections, and the densities were determined using the Archimedes method. For comparison, two *Bovinae* horns from Qinghai yak and domestic cattle were also studied. A small number of transverse orientation samples were also studied to compare with the longitudinal orientation. The results of the other two *Bovinae* horn sheaths and transverse orientation samples are presented in the supplemental information.

Microscale morphology analysis

The microstructure of the *Syncerus caffer* horn sheath was evaluated by X-ray CT (micro-CT, Bruker, SkyScan 2211, Saarbrucken, Germany), using 20 × 2.5 × 2 mm^3 horn samples. The experiment was conducted with a resolution of 5 μm at a 60 kV acceleration voltage and 80 μA current.

Fracture surfaces after tensile and flexural tests were examined using SEM (JSM-6010) under the secondary electron mode at a 20 kV accelerating voltage. The microscale morphology was obtained by immersing the specimens in liquid nitrogen for 3 min and quickly fracturing them. Cross-sections along longitudinal, radial, and transverse directions were all prepared. EDS was utilized for element analysis; for reproducibility, data collection in the same area was repeated ≥ 10 times.

Structure analysis of keratin

FTIR spectra of the horn sheath were collected using an ATR-FTIR spectrometer (Thermo Scientific, Alachua, FL, USA) over a wavenumber range of 700–4,000 cm^{-1} at room temperature (25°C). The peak deconvolution of conformations in the amide I region (1,600–1,700 cm^{-1}) was conducted using PeakFit (v.4.12). The peak type was Gaussian; the peak width at half height (full width at half maximum) was set as 5 cm^{-1}, with the peak positions assigned according to the procedure defined in Cai et al.[8] The sulfur content was also determined by XPS (Thermo Scientific Nexsa) with Al Kα irradiation. TG analysis was conducted on a

DTG-60H (Shimadzu, Japan) with a heating rate of 10°C in air atmosphere from 25°C to 400°C. DSC (DSC25, TA Instruments, New Castle, DE, USA) was tested from 25°C to 200°C at a rate of 20°C min^{-1}. The crystallinity was determined from XRD (Ultima IV Rigaku, Tokyo, Japan).

Mechanical characterization

Uniaxial tensile tests were conducted with dumbbell-shaped specimens on a screw-driven testing machine (Instron 8801, Instron, Norwood, MA, USA), operating at a displacement rate of 2 mm min^{-1}. Due to the small sizes and irregular shapes of natural materials, tensile tests could not be conformed according to standard test method, such as ASTM standard. Instead, the tensile tests were conducted following the cutting dimensions used in Yang et al.[35] Flexural tests were performed on 30 mm long rectangular specimens, 3 mm thick by 8 mm wide, in accordance with ASTM Standard D790-07 using Instron 5565 screw-driven testing machine equipped with a 50 kN load cell. In addition a set of single-edge notched specimens were tested in three-point bending using a displacement rate of 1 mm min^{-1}. The tensile and flexural tests were carried out with pre-loads set at around 1 N. All the samples were cut by water jet cutter. For each test position on the horn sheath, we collected five sets of samples for testing.

The flexural stress and strain were computed using the following formulas:

$$\varepsilon_f = \frac{6Dd}{L^2}, \text{and} \qquad \text{(Equation 1)}$$

$$\sigma_f = \frac{3P \cdot l}{2b \cdot h^2}. \qquad \text{(Equation 2)}$$

Nanoindentation tests were conducted using a Hysitron TI950 Triboindenter equipped with a three-sided pyramidal Berkovich diamond indenter. The load control mode was adopted with a peak load of 25 mN. Five indentations were conducted at each of numerous different positions.

Cohesive finite-element simulation

Cohesive finite-element modeling was conducted under tensile, bending, and drop-weight impact loadings. The modeling was based on a linear elastoplastic constitutive traction separation law determined by a damage initiation criterion, a damage evolution criterion, and a softening law. Models of lamellae structures were constructed and the parameters were set as radius (*R*) and span (S), as shown in Figure 2. The stiffness, strength, and elongation determined by the simulated model were obtained from the experimental tensile properties measured in this study on the proximal part in *Syncerus caffer*. The interfacial adhesion between the lamellae in the *Bovinae* horn sheath was simulated by a cohesive contact. Further details are given in Note S1. On average, we used approximately 50,000 elements in our models. It helped us maintain a balance between computational efficiency and accuracy of our results. Model parameters including modulus, Poisson's ratio, yield strength, ultimate strength, and elongation were set as 2.9 GPa, 0.3, 150 MPa, 180 MPa, and 25%, respectively. Besides, the explicit dynamics solver was adopted.

SUPPLEMENTAL INFORMATION

Supplemental information can be found online at https://doi.org/10.1016/j.xcrp.2023.101576.

ACKNOWLEDGMENTS

The authors are grateful for support from the National Natural Science Foundation of China (nos. 51905019 and 52075528), the Anhui Province University Natural Science Research Project (no. 2022AH050302), the Outstanding Youth Fund of Anhui Province (no. 2108085J22), and the Shenzhen and Hong Kong Joint Innovation Project (no. SGDX2019091716460172).

AUTHOR CONTRIBUTIONS

Conceptualization, K.Y., J.G., and R.O.R.; methodology, K.Y. and R.O.R.; funding acquisition, K.Y., B.W., and S.Z.; formal analysis, K.Y., J.G., Z.W., and W.T.; investigation, K.Y., H.Y., X.C., S.C., Z.Y., N.Q., Z.W., and W.T.; data curation, H.Y.; validation, H.Y.; writing – original & editing, K.Y.; writing – review & editing, K.Y., J.G., W.H., B.W., S.Z., and R.O.R.; supervision, J.G. and R.O.R.; resources, S.Z.

DECLARATION OF INTERESTS

The authors declare no competing interests

INCLUSION AND DIVERSITY

We support inclusive, diverse, and equitable conduct of research.

Received: February 20, 2023
Revised: July 12, 2023
Accepted: August 21, 2023
Published: September 11, 2023

REFERENCES

1. Huang, W., Restrepo, D., Jung, J.Y., Su, F.Y., Liu, Z., Ritchie, R.O., McKittrick, J., Zavattieri, P., and Kisailus, D. (2019). Multiscale Toughening Mechanisms in Biological Materials and Bioinspired Designs. Adv. Mater. *31*, 1901561. https://doi.org/10.1002/adma.201901561.

2. Liu, Z., Meyers, M.A., Zhang, Z., and Ritchie, R.O. (2017). Functional Gradients and Heterogeneities in Biological Materials: Design Principles Functions and Bioinspired Applications. Prog. Mater. Sci. *88*, 467–498. https://doi.org/10.1016/j.pmatsci.2017.04.013.

3. Meyers, M.A., McKittrick, J., and Chen, P.Y. (2013). Structural Biological Materials: Critical Mechanics-Materials Connections. Science *339*, 773–779. https://doi.org/10.1126/science.1220854.

4. Ritchie, R.O. (2011). The conflicts between strength and toughness. Nat. Mater. *10*, 817–822. https://doi.org/10.1038/nmat3115.

5. Zhang, Y., Huang, W., Hayashi, C., Gatesy, J., and McKittrick, J. (2018). Microstructure and Mechanical Properties of Different Keratinous Horns. J. R. Soc. Interface *15*, 20180093. https://doi.org/10.1098/rsif.2018.0093.

6. Zhang, Q., Shan, G., Cao, P., He, J., Lin, Z., Huang, Y., and Ao, N. (2015). Mechanical and Biological Properties of Oxidized Horn Keratin. Mat. Sci. Eng C-Mater. *47*, 123–134. https://doi.org/10.1016/j.msec.2014.11.051.

7. Li, B.W., Zhao, H.P., and Feng, X.Q. (2011). Static and Dynamic Mechanical Properties of Cattle Horns. Mat. Sci. Eng C-Mater. *31*, 179–183. https://doi.org/10.1016/j.msec.2010.08.016.

8. Cai, S., Yang, K., Xu, Y., Guan, J., Han, B., Sun, B., Zeng, Y., and Wu, S. (2021). Structure and Moisture Effect On the Mechanical Behavior of a Natural Biocomposite Buffalo Horn Sheath. Compos. Commun. *26*, 100748. https://doi.org/10.1016/j.coco.2021.100748.

9. Zhang, Q.b., Li, C., Pan, Y.t., Shan, G.h., Cao, P., He, J., Lin, Z.s., Ao, N.j., and Huang, Y.x. (2013). Microstructure and Mechanical Properties of Horns Derived From Three Domestic Bovines. Mat. Sci. Eng C-Mater. *33*, 5036–5043. https://doi.org/10.1016/j.msec.2013.08.034.

10. Johnson, K.L., Trim, M.W., Francis, D.K., Whittington, W.R., Miller, J.A., Bennett, C.E., and Horstemeyer, M.F. (2017). Moisture Anisotropy Stress State and Strain Rate Effects On Bighorn Sheep Horn Keratin Mechanical Properties. Acta Biomater. *48*, 300–308. https://doi.org/10.1016/j.actbio.2016.10.033.

11. Wang, B., Yang, W., McKittrick, J., and Meyers, M.A. (2016). Keratin: Structure Mechanical Properties Occurrence in Biological Organisms and Efforts at Bioinspiration. Prog. Mater. Sci. *76*, 229–318. https://doi.org/10.1016/j.pmatsci.2015.06.001.

12. Yang, K., Qin, N., Zhou, C., Wang, B., Yu, H., Li, H., Yu, H., and Deng, H. (2022). The Study of Mechanical Behaviors of Caprinae Horn Sheath under Pendulum Impact. Polymers *14*, 3272. https://doi.org/10.3390/polym14163272.

13. Huang, W., Zaheri, A., Yang, W., Kisailus, D., Ritchie, R.O., Espinosa, H., and McKittrick, J. (2019). How Water Can Affect Keratin: Hydration-Driven Recovery of Bighorn Sheep (*Ovis Canadensis*) Horns. Adv. Funct. Mater. *29*, 1901077. https://doi.org/10.1002/adfm.201901077.

14. Fuller, L.H., and Donahue, S.W. (2021). Material Properties of Bighorn Sheep (*Ovis Canadensis*) Horncore Bone with Implications for Energy Absorption During Impacts. J. Mech. Behav. Biomed. *114*, 104224. https://doi.org/10.1016/j.jmbbm.2020.104224.

15. Liu, S., Xu, S., Song, J., Zhou, J., Xu, L., Li, X., and Zou, M. (2020). Mechanical Properties and Failure Deformation Mechanisms of Yak Horn Under Quasi-Static Compression and Dynamic Impact. J. Mech. Behav. Biomed. *107*, 103753. https://doi.org/10.1016/j.jmbbm.2020.103753.

16. Zhou, J., Liu, S., Guo, Z., Xu, S., Song, J., and Zou, M. (2022). Study On the Energy Absorption Performance of Bionic Tube Inspired by Yak Horn. Mech. Adv. Mater. Struct. *29*, 7246–7258. https://doi.org/10.1080/15376494.2021.1995088.

17. Sun, J., Wu, W., Xue, W., Tong, J., and Liu, X. (2016). Anisotropic nanomechanical properties of bovine horn using modulus mapping. IET. Nanbiotechnol. *10*, 334–339. https://doi.org/10.1049/iet-nbt.2015.0082.

18. Kitchener, A. (1987). Fracture toughness of horns and a reinterpretation of the horning behaviour of bovids. J. Zool. *213*, 621–639.

https://doi.org/10.1111/j.1469-7998.1987.tb03730.x.

19. Kitchener, A., and Vincent, J.F.V. (1987). Composite Theory and the Effect of Water On the Stiffness of Horn Keratin. J. Mater. Sci. *22*, 1385–1389. https://doi.org/10.1007/BF01233138.

20. Wei, H. (2018). Impact Resistant and Energy Absorbent Natural Keratin Materials: Horns and Hooves. PHD Thesis (University of California San Diego). https://escholarship.org/uc/item/4kn4z9dp.

21. Xu, J., Li, Y., and Fu, K. (2022). Impact Resistance of Horn-Inspired Tubular Composite Structure. Acta Mater. Compos. Sin. *40*, 1–12. https://doi.org/10.13801/j.cnki.fhclxb.20220530.006.

22. Tombolato, L., Novitskaya, E.E., Chen, P.Y., Sheppard, F.A., and McKittrick, J. (2010). Microstructure, Elastic Properties and Deformation Mechanisms of Horn Keratin. Acta Biomater. *6*, 319–330. https://doi.org/10.1016/j.actbio.2009.06.033.

23. Hieronymus, T.L., Witmer, L.M., and Ridgely, R.C. (2006). Structure of white rhinoceros (*Ceratotherium simum*) horn investigated by X-ray computed tomography and histology with implications for growth and external form. J. Morphol. *267*, 1172–1176. https://doi.org/10.1002/jmor.10465.

24. Huang, W., Yaraghi, N.A., Yang, W., Velazquez-Olivera, A., Li, Z., Ritchie, R.O., Kisailus, D., Stover, S.M., and McKittrick, J. (2019). Natural Energy Absorbent Polymer Composite: The Equine Hoof Wall. Acta Biomater. *90*, 267–277. https://doi.org/10.1016/j.actbio.2019.04.003.

25. Launey, M.E., Chen, P.Y., Mckittrick, J., and Ritchie, R.O. (2010). Mechanistic aspects of the fracture toughness of elk antler bone. Acta Biomater. *6*, 1505–1514. https://doi.org/10.1016/j.actbio.2009.11.026.

26. Imbeni, V., Kruzic, J.J., Marshall, G.W., Marshall, S.J., and Ritchie, R.O. (2005). The dentin-enamel junction and the fracture of human teeth. Nat. Mater. *4*, 229–232. https://doi.org/10.1038/nmat1323.

27. Kasapi, M.A., and Gosline, J.M. (1999). Micromechanics of the equine hoof wall: optimizing crack control and material stiffness through modulation of the properties of keratin. J. Exp. Biol. *202*, 377–391. https://doi.org/10.1242/jeb.202.4.377.

28. Li, B.W., Zhao, H.P., Feng, X.Q., Guo, W.W., and Shan, S.C. (2010). Experimental Study On the Mechanical Properties of the Horn Sheaths From Cattle. J. Exp. Biol. *213*, 479–486. https://doi.org/10.1242/jeb.035428.

29. Raut, H.K., Schwartzman, A.F., Das, R., Liu, F., Wang, L., Ross, C.A., and Fernandez, J.G. (2020). Tough and Strong: Cross-Lamella Design Imparts Multifunctionality to Biomimetic Nacre. ACS Nano *14*, 9771–9779. https://doi.org/10.1021/acsnano.0c01511.

30. Yaraghi, N.A., Guarín-Zapata, N., Grunenfelder, L.K., Hintsala, E., Bhowmick, S., Hiller, J.M., Betts, M., Principe, E.L., Jung, J.Y., Sheppard, L., et al. (2016). A Sinusoidally Architected Helicoidal Biocomposite. Adv. Mater. *28*, 6835–6844. https://doi.org/10.1002/adma.201600786.

31. Espinosa, H.D., Juster, A.L., Latourte, F.J., Loh, O.Y., Gregoire, D., and Zavattieri, P.D. (2011). Tablet-level origin of toughening in abalone shells and translation to synthetic composite materials. Nat. Commun. *2*, 173. https://doi.org/10.1038/ncomms1172.

32. Amorim, L., Santos, A., Nunes, J.P., and Viana, J.C. (2021). Bioinspired approaches for toughening of fibre reinforced polymer composites. Mater. Des. *199*, 109336. https://doi.org/10.1016/j.matdes.2020.109336.

33. Nguyen-Van, V., Wickramasinghe, S., Ghazlan, A., Nguyen-Xuan, H., and Tran, P. (2020). Uniaxial and biaxial bioinspired interlocking composite panels subjected to dynamic loadings. Thin-Walled Struct. *157*, 107023. https://doi.org/10.1016/j.tws.2020.107023.

34. Drake, A., Haut Donahue, T.L., Stansloski, M., Fox, K., Wheatley, B.B., and Donahue, S.W. (2016). Horn and Horn Core Trabecular Bone of Bighorn Sheep Rams Absorbs Impact Energy and Reduces Brain Cavity Accelerations During High Impact Ramming of the Skull. Acta Biomater. *44*, 41–50. https://doi.org/10.1016/j.actbio.2016.08.019.

35. Yang, K., Qin, N., Yu, H., Zhou, C., Deng, H., Tian, W., Cai, S., Wu, Z., and Guan, J. (2022). Correlating multi-scale structure characteristics to mechanical behavior of Caprinae horn sheaths. J. Mater. Res. Technol. *21*, 2191–2202. https://doi.org/10.1016/j.jmrt.2022.10.044.

36. Yang, K., Yazawa, K., Tsuchiya, K., Numata, K., and Guan, J. (2019). Molecular Interactions and Toughening Mechanisms in Silk Fibroin-Epoxy Resin Blend Films. Biomacromolecules *20*, 2295–2304. https://doi.org/10.1021/acs.biomac.9b00260.

37. Yang, K., Wu, Z., Zhou, C., Cai, S., Wu, Z., Tian, W., Wu, S., Ritchie, R.O., and Guan, J. (2022). Comparison of toughening mechanisms in natural silk-reinforced composites with three epoxy resin matrices. Compos. Part A-Appl. S. *154*, 106760. https://doi.org/10.1016/j.compositesa.2021.106760.

38. Aguirre, T.G., Fuller, L., Ingrole, A., Seek, T.W., Wheatley, B.B., Steineman, B.D., Donahue, T.L.H., and Donahue, S.W. (2020). Bioinspired Material Architectures From Bighorn Sheep Horncore Velar Bone for Impact Loading Applications. Sci. Rep. *10*, 18916. https://doi.org/10.1038/s41598-020-76021-5.

39. Johnson, K.L., Trim, M.W., Horstemeyer, M.F., Lee, N., Williams, L.N., Liao, J., Rhee, H., and Prabhu, R. (2014). Geometric Effects on Stress Wave Propagation. J. Biomech. Eng. *136*, 021023. https://doi.org/10.1115/1.4026320.

40. Maity, P., and Tekalur, S.A. (2011). Biomechanical Analysis of Ramming Behavior in *Ovis Canadensis*. Springer *3*, 357–364. https://doi.org/10.1007/978-1-4419-9794-4_50.

41. Yang, K., Guan, J., Numata, K., Wu, C., Wu, S., Shao, Z., and Ritchie, R.O. (2019). Integrating tough Antheraea pernyi silk and strong carbon fibres for impact-critical structural composites. Nat. Commun. *10*, 3786. https://doi.org/10.1038/s41467-019-11520-2.

42. Bragulla, H.H., and Homberger, D.G. (2009). Structure and functions of keratin proteins in simple, stratified, keratinized and cornified epithelia. J. Anat. *214*, 516–559. https://doi.org/10.1111/j.1469-7580.2009.01066.x.

43. Tomlinson, D.J., Mülling, C.H., and Fakler, T.M. (2004). Invited Review: Formation of Keratins in the Bovine Claw: Roles of Hormones, Minerals, and Vitamins in Functional Claw Integrity. J. Dairy Sci. *87*, 797–809. https://doi.org/10.3168/jds.S0022-0302(04)73223-3.

44. Chen, J.H., Liu, C., You, L., and Simmons, C.A. (2010). Boning up on Wolff's Law: Mechanical regulation of the cells that make and maintain bone. J. Biomech. *43*, 108–118. https://doi.org/10.1016/j.jbiomech.2009.09.016.

45. Wolff, J. (2010). The Classic: On the Inner Architecture of Bones and its Importance for Bone Growth. Clin. Orthop. Relat. Res. *468*, 1056–1065. https://doi.org/10.1007/s11999-010-1239-2.

46. Xin, A., Su, Y., Feng, S., Yan, M., Yu, K., Feng, Z., Hoon Lee, K., Sun, L., and Wang, Q. (2021). Growing Living Composites with Ordered Microstructures and Exceptional Mechanical Properties. Adv. Mater. *33*, 2006946. https://doi.org/10.1002/adma.202006946.

47. Yang, L., Wu, Y., Yang, F., Wu, X., Cai, Y., and Zhang, J. (2021). A wood textile fiber made from natural wood. J. Mater. Sci. *56*, 15122–15133. https://doi.org/10.1007/s10853-021-06240-2.

48. Guan, Q.F., Han, Z.M., Yang, H.B., Ling, Z.C., and Yu, S.H. (2021). Regenerated isotropic wood. Natl. Sci. Rev. *8*, nwaa230. https://doi.org/10.1093/nsr/nwaa230.

49. Yang, K., Guan, J., Shao, Z., and Ritchie, R.O. (2020). Mechanical properties and toughening mechanisms of natural silkworm silks and their composites. J. Mech. Behav. Biomed. *110*, 103942. https://doi.org/10.1016/j.jmbbm.2020.103942.

50. Yu, Y., Yang, W., Wang, B., and Meyers, M.A. (2017). Structure and mechanical behavior of human hair. Mater. Sci. Eng. C *73*, 152–163. https://doi.org/10.1016/j.msec.2016.12.008.

51. Kunchi, C., Venkateshan, K.C., and Adusumalli, R.B. (2018). Effect of Scalp Position on Tensile Properties of Single Hair Fibers. Int. J. Trichol. *10*, 218–228. https://doi.org/10.4103/ijt.ijt_19_18.

52. Arola, D.D., and Reprogel, R.K. (2006). Tubule orientation and the fatigue strength of human dentin. Biomaterials *27*, 2131–2140. https://doi.org/10.1016/j.biomaterials.2005.10.005.

53. Liang, S.M., Ji, H.M., and Li, X.W. (2020). Thickness-dependent mechanical properties of nacre in Cristaria plicata shell: Critical role of interfaces. J. Mater. Sci. Technol. *44*, 1–8. https://doi.org/10.1016/j.jmst.2019.10.039.

54. Barthelat, F., Li, C.M., Comi, C., and Espinosa, H.D. (2006). Mechanical properties of nacre constituents and their impact on mechanical performance. J. Mater. Res. *21*, 1977–1986. https://doi.org/10.1557/jmr.2006.0239.

55. Chen, G., Luo, H., Wu, S., Guan, J., Luo, J., and Zhao, T. (2018). Flexural deformation and fracture behaviors of bamboo with gradient hierarchical fibrous structure and water content. Compos. Sci. Technol. *157*, 126–133. https://doi.org/10.1016/j.compscitech.2018.01.034.

56. Dixon, P.G., and Gibson, L.J. (2014). The structure and mechanics of Moso bamboo material. J. R. Soc. Interface *11*, 20140321. https://doi.org/10.1098/rsif.2014.0321.

57. Ritchie, R.O., Cannon, R.M., Dalgleish, B.J., Dauskardt, R.H., and McNaney, J.M. (1993). Mechanics and Mechanisms of Crack Growth at or Near Ceramic-Metal Interfaces: Interface Engineering Strategies for Promoting Toughness. Mater. Sci. Eng. *166*, 221–235. https://doi.org/10.1016/0921-5093(93)90325-9.

58. Barthelat, F., Tang, H., Zavattieri, P., Li, C., and Espinosa, H. (2007). On the Mechanics of Mother-of-Pearl: A Key Feature in the Material Hierarchical Structure. J. Mech. Phys. Solid. *55*, 306–337. https://doi.org/10.1016/j.jmps.2006.07.007.

59. Barthelat, F., Yin, Z., and Buehler, M.J. (2016). Structure and Mechanics of Interfaces in Biological Materials. Nat. Rev. Mater. *1*, 16007. https://doi.org/10.1038/natrevmats.2016.7.

60. Rivera, J., Hosseini, M.S., Restrepo, D., Murata, S., Vasile, D., Parkinson, D.Y., Barnard, H.S., Arakaki, A., Zavattieri, P., and Kisailus, D. (2020). Toughening Mechanisms of the Elytra of the Diabolical Ironclad Beetle. Nature *586*, 543–548. https://doi.org/10.1038/s41586-020-2813-8.

61. Garner, S.N., Naleway, S.E., Hosseini, M.S., Acevedo, C., Gludovatz, B., Schaible, E., Jung, J.Y., Ritchie, R.O., Zavattieri, P., and McKittrick, J. (2020). The Role of Collagen in the Dermal Armor of the Boxfish. J. Mater. Res. Technol. *9*, 13825–13841. https://doi.org/10.1016/j.jmrt.2020.09.090.

62. Zhang, Y., Zhao, H., Deng, B., Basu, S., Huang, L., and Shi, Y. (2021). Design Ductile and Work-Hardenable Composites with All Brittle Constituents. Acta Mater. *208*, 116770. https://doi.org/10.1016/j.actamat.2021.116770.

63. Xia, S., Wang, Z., Chen, H., Fu, W., Wang, J., Li, Z., and Jiang, L. (2015). Nanoasperity: Structure Origin of Nacre-Inspired Nanocomposites. ACS Nano *9*, 2167–2172. https://doi.org/10.1021/acsnano.5b00119.

64. Lee, S., Novitskaya, E.E., Reynante, B., Vasquez, J., Urbaniak, R., Takahashi, T., Woolley, E., Tombolato, L., Chen, P.Y., and McKittrick, J. (2011). Impact testing of structural biological materials. Mater. Sci. Eng. C *31*, 730–739. https://doi.org/10.1016/j.msec.2010.10.017.